Junjie Zhu
Xiangchun Xuan

Department of Mechanical Engineering, Clemson University, Clemson, SC, USA

Received January 9, 2009
Revised April 13, 2009
Accepted April 14, 2009

Research Article

Dielectrophoretic focusing of particles in a microchannel constriction using DC-biased AC flectric fields

This paper presents a fundamental study of particle electrokinetic focusing in a single microchannel constriction. Through both experiments and simulations, we demonstrate that such dielectrophoresis-induced particle focusing can be implemented in a much smaller magnitude of DC-biased AC electric fields (10 kV/m in total) as compared to pure DC electric fields (up to 100 kV/m). This is attributed to the increase in the ratio of cross-stream particle dielectrophoretic velocity to streamwise electrokinetic velocity as only the DC field component contributes to the latter. The effects of the 1 kHz frequency AC to DC electric field ratio on particle trajectories and velocity variations through the microchannel constriction are also examined, which are found to agree with the simulation results.

Keywords:
DC-biased AC electric field / Dielectrophoresis / Electrokinetic flow / Microchannel constriction / Particle focusing

DOI 10.1002/elps.200900017

1 Introducton

Lab-on-a-chip devices have been increasingly used to manipulate microparticles (both biological and synthetic) over the past decade [1–3]. Particle focusing is a fundamental operation in many such microfluidic particle-handling devices. In this operation, dispersed particles are focused to a tight stream enabling subsequent detection and sorting [4–6]. Microfluidic particle focusing has been realized primarily by using hydrodynamic [7–10] or electrokinetic [11–15] sheath flow(s) to pinch the suspending medium and thus focus particles. Other than this flow-assisted method, a variety of sheathless focusing approaches have also been demonstrated. For example, particle focusing has been achieved by applying an external force field, such as optical [16], acoustic [17], electrophoretic [18], and AC dielectrophoretic [19–22], to manipulate particles directly to their equilibrium positions in the pressure-pumping particulate stream. In addition, particle focusing has also been achieved by using hydrodynamic filtration [23, 24], hydrophoresis [25, 26], DC dielectrophoresis [27], and inertia [28–31] *etc*.

Correspondence: Professor Xiangchun Xuan, Department of Mechanical Engineering, Clemson University, Clemson, SC 29634-0921, USA
E-mail: xcxuan@clemson.edu
Fax: +1-864-656-7299

This article presents an experimental and numerical study of dielectrophoretic focusing of particles in a microchannel constriction using DC-biased AC electric fields. We acknowledge that the DC dielectrophoretic focusing of particles has been suggested and studied in constrictions formed by an array or pairs of insulating micro-obstacles such as oil menisci [27, 32, 33]. In these works, however, it is necessary that either the particle size is comparable with the constriction width or the applied DC electric field is sufficiently large. The former condition increases the probability of particle clogging and chip fouling, and the latter condition may pose problems to cell viability *via* the transmembrane voltage and Joule heating, particularly significant within the constrictions [34]. For example, it has been reported that the locally amplified electric field could cause temperature rises in the constrictions due to Joule heating and thus damages to cells or disturbances to particle motions [35, 36]. Additionally, microchannels with constrictions have also been employed to realize DC dielectrophoretic trapping and separation of particles and cells [37–43].

We demonstrate in this work that using DC-biased AC electric fields can significantly improve the particle focusing performance in a microchannel constriction, so that the required magnitude of electric field can be reduced considerably. It is noted that DC-biased AC electric fields have recently been used to improve the dielectrophoretic trapping and/or the separation of particles in microchannels with a

constriction in the channel depth [44] and width [45] directions, respectively.

2 Theoretical background

Figure 1 shows the electric field lines (with arrows indicating the directions in the top plot) and the contour of electric field intensity (the darker the higher) in a microchannel constriction. As the electric field becomes non-uniform, particles experience variable dielectrophoretic forces, $\boldsymbol{F}_{\mathrm{DEP}}$ (bold symbol denotes a vector hereafter), when they move electrokinetically through the constriction. Using the dipole moment approximation, $\boldsymbol{F}_{\mathrm{DEP}}$ on an isolated spherical particle in DC fields is given by [46]

$$\mathbf{F}_{\mathrm{DEP}} = (1/2)\pi\varepsilon_f d^3 f_{\mathrm{CM}}(\mathbf{E}\cdot\nabla\mathbf{E}) \tag{1}$$

$$f_{\mathrm{CM}} = \left(\sigma_p - \sigma_f\right)/\left(\sigma_p + 2\sigma_f\right) \tag{2}$$

where ε_f is the fluid permittivity, d the particle diameter, f_{CM} the Clausius-Mossotti (CM) factor, $\mathbf{E}$ the DC electric field strength, σ_p the electric conductivity of particles, and σ_f the electric conductivity of the suspending fluid. It is important to note that Eq. (1) is valid only when the particle size is much smaller than the characteristic length scale of the electric field [46]. Apparently, this condition may break down when particles approach the constriction. Therefore, we will introduce a correction factor in the Modeling section to account for the size effects on particle dielectrophoresis (see Section 4).

In DC and low-frequency AC electric fields (<100 kHz), live biological cells [34] and polystyrene particles [47] often appear insulating, *i.e.* $\sigma_p<\sigma_f$, and so $f_{\mathrm{CM}}<0$ leading to a negative dielectrophoresis. In other words, $\boldsymbol{F}_{\mathrm{DEP}}$ is directed towards the lower electric field region as indicated in Fig. 1. By balancing $\boldsymbol{F}_{\mathrm{DEP}}$ with the Stokes drag force, one can obtain the dielectrophoretic particle velocity, $\boldsymbol{U}_{\mathrm{DEP}}$, which is then superimposed to electrokinetic flow (a combination of fluid electroosmosis and particle electrophoresis), $\boldsymbol{U}_{\mathrm{EK}}$, to get the real particle velocity, $\mathbf{U}_p$, *i.e.*

$$\mathbf{U}_p = \mathbf{U}_{\mathrm{EK}} + \mathbf{U}_{\mathrm{DEP}} = \mu_{\mathrm{EK}}\mathbf{E} + \mu_{\mathrm{DEP}}(\mathbf{E}\cdot\nabla\mathbf{E}) \tag{3}$$

$$\mu_{\mathrm{DEP}} = \varepsilon_f d^2 f_{\mathrm{CM}}/6\mu_f \tag{4}$$

where μ_{EK} is the electrokinetic mobility, μ_{DEP} the dielectrophoretic mobility which is negative as $f_{\mathrm{CM}}<0$, and μ_f the fluid viscosity.

Essentially there exist two sources of electric field non-uniformities in the channel constriction region (see Fig. 1): one is due to the reduction of cross-sectional area in the constriction, which gives rise to electric field gradients primarily along the direction of electric field lines, and the other is due to the singularity around corners of the constriction, which causes electric field gradients mainly normal to the direction of electric field lines. As a matter of fact, the electric field lines in electrokinetic flows are equivalent to their streamlines due to the similarity between

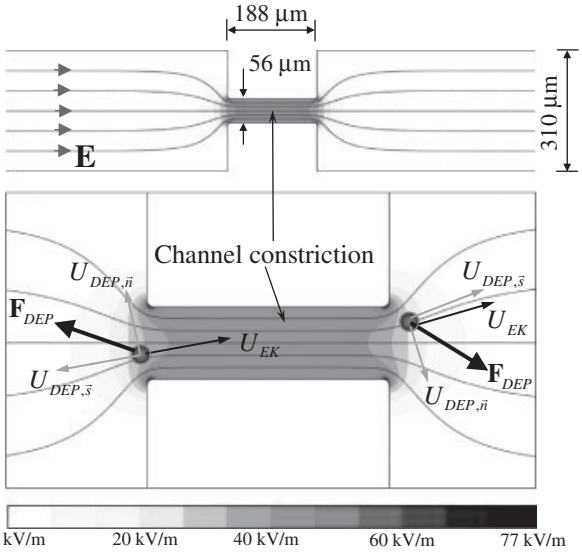

Figure 1. Illustration of the DC dielectrophoretic focusing (see the velocity analyses of the two particles, bottom plot) of particles in a microchannel constriction. The top plot displays the zoom-out view of the constriction with the measured channel dimensions indicated. In both plots, the background shows the simulated electric field intensity (the darker the higher, see legend) and the arrowed curves indicate the electric field lines. The total length of the channel is 2 cm, across which a total voltage drop (DC plus RMS AC) of 200 V or an average electric field of 10 kV/m has been imposed.

electroosmotic flow and electric fields [48]. Hence, we may conveniently express the particle velocity, $\mathbf{U}_p$ in Eq. (3), in terms of streamline coordinates (see Fig. 1, bottom plot),

$$\begin{aligned}\mathbf{U}_p &= \left(U_{\mathrm{EK}} + U_{\mathrm{DEP},\vec{s}}\right)\hat{\mathbf{s}} + U_{\mathrm{DEP},\vec{n}}\hat{\mathbf{n}} \\ &= \left(\mu_{\mathrm{EK}}E + \mu_{\mathrm{DEP}}E\frac{\partial E}{\partial s}\right)\hat{\mathbf{s}} + \mu_{\mathrm{DEP}}\frac{E^2}{\Re}\hat{\mathbf{n}}\end{aligned} \tag{5}$$

where U_{EK} is the streamwise electrokinetic velocity, $U_{\mathrm{DEP},\vec{s}}$ the dielectrophoretic particle velocity in the streamline direction with the unit vector $\hat{\mathbf{s}}$, $U_{\mathrm{DEP},\vec{n}}$ the dielectrophoretic particle velocity normal to the streamline direction with the unit vector $\hat{\mathbf{n}}$, E the electric field intensity, and $\Re$ the radius of curvature of the streamline, which is mainly dependent on the dimensions of the channel constriction.

As noted earlier, particles undertake negative dielectrophoresis, and so $U_{\mathrm{DEP},\vec{n}}$ points towards the channel centerline on both sides of the constriction, indicating a particle focusing effect as illustrated in Fig. 1 (see the velocity analyses of both particles in the bottom plot). The efficiency of this focusing is determined by the ratio of the distance a particle moves perpendicular to the streamline to the distance traveled along the streamline. This ratio is equivalent to the ratio of particle velocity perpendicular and parallel to the streamline,

$$\frac{U_{\mathrm{DEP},\vec{n}}}{U_{\mathrm{EK}} + U_{\mathrm{DEP},\vec{s}}} = \left(\frac{\mu_{\mathrm{DEP}}}{\mu_{\mathrm{EK}} + \mu_{\mathrm{DEP}}\partial E/\partial s}\right)\frac{E}{\Re} \tag{6}$$

Considering the negative dielectrophoretic mobility μ_{DEP}, it is straightforward to see that this velocity ratio and thus the efficiency of dielectrophoretic particle focusing increase with the rise of electric field.

As to $U_{DEP,\vec{s}}$, it is against U_{EK} in the upstream of the constriction and thus slows down the incoming particles, see the velocity analysis of the particle on the left in Fig. 1 (bottom plot). Moreover, since $U_{DEP,\vec{s}}$ is a second-order function of electric field, while U_{EK} is only a linear function, see Eq. (3), it is likely that $U_{DEP,\vec{s}}$ counter-balances U_{EK} at large electric fields and so particles are stagnated and concentrated ahead of the constriction. This phenomenon has been observed previously [32, 37–41, 49]. In the downstream of the constriction, however, particles gain a propelling force from dielectrophoresis because $U_{DEP,\vec{s}}$ is in the same direction as U_{EK}, see the velocity analysis of the particle on the right in Fig. 1 (bottom plot). Therefore, one may expect an extreme point in particle velocity on the rear side of the constriction if $U_{DEP,\vec{s}}$ is large enough to compensate the decrease in U_{EK} as a consequence of decrease in the local electric field.

If, instead, DC-biased AC electric fields are used for **E** (or *E*) in the above equations, we have

$$\mathbf{E} = \mathbf{E}_{DC} + \mathbf{E}_{AC} = \mathbf{E}_{DC}(1+\alpha) \tag{7}$$

where $\mathbf{E}_{DC}$ is the DC electric field strength, $\mathbf{E}_{AC}$ the root-mean-square (RMS) value of the AC electric field strength, and α the ratio of $\mathbf{E}_{AC}$ to $\mathbf{E}_{DC}$. It is straightforward that **E** becomes a pure DC field when $\alpha = 0$. As the time-averaged AC dielectrophoretic velocity shares the same form as DC dielectrophoretic velocity and only the DC field component produces electrokinetic flow, the particle velocity in Eqs. (3) and (5) are, respectively, rewritten as

$$\mathbf{U}_p = \mu_{EK}\mathbf{E}_{DC} + \mu_{DEP}(1+\alpha)^2(\mathbf{E}_{DC}\cdot\nabla\mathbf{E}_{DC}) \tag{8}$$

$$\mathbf{U}_p = \left[\mu_{EK}E_{DC} + \mu_{DEP}(1+\alpha)^2 E_{DC}\frac{\partial E_{DC}}{\partial s}\right]\hat{\mathbf{s}} + \mu_{DEP} \times (1+\alpha)^2\frac{E_{DC}^2}{\Re}\hat{\mathbf{n}} \tag{9}$$

Note that the CM factor (and thus the dielectrophoretic mobility μ_{DEP}) for particles in low-frequency AC electric fields (1 kHz was used in our experiments) has been assumed to be approximately the same as that in DC fields, see Eq. (2). The particle velocity ratio for dielectrophoretic focusing, *i.e.* Eq. (6), is thus rewritten as

$$\frac{U_{DEP,\vec{n}}}{U_{EK}+U_{DEP,\vec{s}}} = \left[\frac{\mu_{DEP}(1+\alpha)^2}{\mu_{EK}+\mu_{DEP}(1+\alpha)^2\partial E_{DC}/\partial s}\right]\frac{E_{DC}}{\Re} \tag{10}$$

For the sake of fair comparisons, we maintain the total RMS magnitude of electric field at E_0, while the AC to DC electric field ratio α is allowed to vary from 0 (*i.e.* a pure DC field) to any positive value (*i.e.* a DC-biased AC field), that is to say,

$$(1+\alpha)E_{DC} = E_0 \tag{11}$$

Hence, Eq. (10) is rearranged as

$$\frac{U_{DEP,\vec{n}}}{U_{EK}+U_{DEP,\vec{s}}} = \left[\frac{\mu_{DEP}(1+\alpha)}{\mu_{EK}+\mu_{DEP}(1+\alpha)\partial E_0/\partial s}\right]\frac{E_0}{\Re} \tag{12}$$

One can see that particle focusing is enhanced by at least α folds in DC-biased AC electric fields as compared with the pure DC electric field. Or alternatively, the necessary magnitude of electric field, E_0, to implement a similar particle focusing will be dramatically smaller in DC-biased AC electric fields.

3 Materials and methods

3.1 Chemicals

SU-8 photoresist (formulation 25) and developer were purchased from MicroChem (Newton, MA). Isopropyl alcohol was obtained from Sigma-Aldrich (St. Louis, MO). Liquid Polydimethylsiloxane (PDMS) was prepared by thoroughly mixing Sylgard 184 and its curing agent (Dow Corning, Midland, MI) at a 10:1 ratio in weight. Polystyrene particles of 5 μm and 10 μm in diameter were purchased from Sigma-Aldrich in the form of 10% solid suspension in water. Their calculated electric conductivities, *i.e.* σ_p in Eq. (2), are 8.96 μS/cm and 4.48 μS/cm, respectively, if the surface conductance is assumed to be 1 nS as suggested by Ermolina and Morgan [47]. Both particles were re-suspended in 1 mM KCl solution at a volume ratio of 1:200 and 1:50, respectively. The measured electric conductivity of the solution, *i.e.* σ_f in Eq. (2), is about 160 μS/cm. Therefore, the CM factor, *i.e.* f_{CM} as defined in Eq. (2), was determined as −0.46 and −0.48 for 5 μm and 10 μm particles, respectively.

3.2 Microchannel fabrication

The microchannel was fabricated in PDMS using the standard soft lithography technique [50]. The channel layout was drawn in AutoCAD, and printed onto a transparent thin film at a resolution of 10 000 dpi (CAD/Art Services, Bandon, OR) serving as the photomask. Photoresist was spin-coated (WS-400E-NPP-Lite, Laurell Technologies, North Wales, PA) onto a clean glass slide at a terminal speed of 2000 rpm, yielding a nominal film thickness of 25 μm. After a two-step soft bake (65°C for 3 min and 95°C for 7 min) on hotplates (HP30A, Torrey Pines Scientific, San Marcos, CA), the photoresist film was exposed to near UV light (ABM, San Jose, CA) through the negative photomask. Following another two-step hard bake (65°C for 1 minu and 95°C for 3 min), the photoresist was developed in SU-8 developer solution for 4 min, the result of which was a positive replica of the microchannel on the glass slide. After a brief rinse with isopropyl alcohol and a final hard bake at 150°C for 5 min, the cured photoresist was ready for use as the mold of the microchannel constriction.

Liquid PDMS was then poured over the channel mold that settled in a Petri dish. After a 30 min degassing in an isotemp vacuum oven (13-262-280A, Fisher Scientific, Fair Lawn, NJ), liquid PDMS was cured at 70°C in a gravity

convection oven (13-246-506GA, Fisher Scientific) for 1–2 h. Subsequently, the PDMS that encloses the entire microchannel was cut using a scalpel and peeled off from the mold. Two through holes were punched in the PDMS cast to serve as reservoirs. Then, the channel side of the PDMS was plasma treated (PDC-32G, Harrick Scientific, Ossining, NY) for 1 min along with a clean glass slide. Immediately following that, the two treated surfaces were bonded irreversibly to form the microchannel. After sealing, the working buffer was introduced into the channel by capillary action in order to prime the channel and maintain the wall surface properties.

The microchannel we fabricated is 2 cm long with a measured width of 310 μm. The constriction is right in the middle of the channel with a measured width of 56 μm and a measured length of 188 μm, see Fig. 1 (top). The whole channel has a uniform depth of 25 μm as noted above.

3.3 Experimental technique

The dielectrophoretic focusing of particles in the microchannel constriction was implemented by imposing either pure DC or DC-biased AC electric fields across the channel. Both electric fields were generated by a function generator (33220A, Agilent Technologies, Santa Clara, CA) in conjunction with a high-voltage amplifier (609E-6, Trek, Medina, NY). Our amplifier is able to amplify AC voltages of up to 6 kHz frequency with 1% distortion. Within this frequency range, we didn't observe a noticeable difference in particle focusing. Therefore, the AC field frequency was fixed to 1 kHz in our experiments. In the pure DC case, the magnitude of average electric field was varied from 10 to 100 kV/m. Note that the electric field intensity at the centerline of the constriction is about 5.5 ($=310\,\mu m/56\,\mu m$) times the average electric field across the whole microchannel, and that at the corners of the constriction reaches a even higher value (see legend in Fig. 1 where an average electric field of 10 kV/m has been imposed). In the DC-biased AC case, the total magnitude of AC and DC electric fields was fixed at 10 kV/m while their ratio was allowed to vary from one to nine. Pressure-driven particle motions were eliminated by carefully balancing the liquid heights in the two reservoirs prior to each measurement.

Particle behaviors through the microchannel constriction were visualized through an inverted microscope (Nikon Eclipse TE2000U, Nikon Instruments, Lewisville, TX) and recorded using a CCD camera (Nikon DS-Qi1Mc). The camera was run in the video mode at a maximum rate of 19 frames *per* second. The acquired digital images had a resolution of 640×512 pixels, corresponding to a 942 μm visible channel length under a $10\times$ objective. All videos and images were re-processed in the Nikon imaging software (NIS-Elements AR 2.30), from which the pixel information of particle center positions with respect to time was extracted manually. This particle center information was then used to determine the particle velocity by dividing the distance the particle center translated between neighboring images over the corresponding time interval. Particle streak images were obtained by superimposing the consecutive images in a video run which typically lasted for 30 s.

4 Modeling

In order to predict the observed particle focusing behaviors, we developed a numerical model in COMSOL 3.3 (Burlington, MA) to simulate the electric field-mediated particle transport through the microchannel constriction. This model is based on that developed by Kang *et al.* [42, 49]. For simplicity, the perturbations of particles on the flow and electric fields (*via* moving boundaries in both fields due to the finite particle size) were neglected in the model, so were the particle–particle interactions. Instead, a correction factor, c as mentioned earlier in Section 2.1, was introduced to account for the effects of particle size (and others if any) on the dielectrophoretic velocity. Hence, the particle velocity in Eq. (8) is revised as

$$\mathbf{U}_p = \mu_{EK}\mathbf{E}_{DC} + c\mu_{DEP}(1+\alpha)^2(\mathbf{E}_{DC}\cdot\nabla\mathbf{E}_{DC}) \qquad (13)$$

Intuitively c should increase with decreasing particle size and approach 1 for point-like particles.

As to the effects of particle size on electrokinetic velocity, they have all been lumped into the electrokinetic mobility, μ_{EK}. It is well known that μ_{EK} is a complex function of the properties of the microchannel-solution-particle system, but insensitive to the particle size and channel width as long as their ratio is kept small [51, 52]. In our experiments, the largest ratio of particle diameter to channel width occurs in the constriction for 10 μm particles and is less than 0.2. Based on Keh and Anderson's analysis [53] and our earlier experiment [33], we find that μ_{EK} should vary no more than 1% throughout the whole channel. Therefore, μ_{EK} was determined by measuring the average particle velocity in the region far away from the constriction where particle dielectrophoresis is negligible. We obtained an almost equal value of $\mu_{EK} = 6.0\times10^{-8}\,m^2/(V\cdot s)$ for the 5 and 10 μm particles used in our experiments with an estimated error of 10%. It is acknowledged that the accuracy of μ_{EK} measurement may be affected by the channel constriction in two aspects: one is that the real electric field in the measuring region is slightly smaller than the average electric field due to the large electrical resistance within the constriction, and the other is that the measured particle velocity is slightly different from the real electrokinetic velocity due to the constriction-induced pressure-driven flow. However, we found through numerical modeling that both effects are negligible as the length of the constriction (188 μm) is far smaller than that of the channel (2 cm). The particle velocity in Eq. (13) was used in a particle tracing function in COMSOL (Burlington) to compute the particle trajectory. Particles were assumed massless and uniformly distributed at the channel inlet. As particle dielectrophoresis happens only in the channel width direction (note: particles

were moving close to the bottom wall of the rectangular channel due to their slightly larger density than the suspending medium, and the particle lift was negligible in our experiment), a 2-D model was employed to predict the particle focusing behaviors without considering the effects of the top and bottom channel walls on particle motions. This treatment has been proved reasonable in predicting particle trajectories in our recent studies as long as the channel has a uniform depth [42, 49].

In the simulation, the dielectrophoretic mobility, μ_{DEP}, was calculated directly from Eq. (4) with the typical dynamic viscosity, $\mu = 0.9 \times 10^{-3}$ kg/(m s), and permittivity, $\varepsilon_f = 6.9 \times 10^{-10}$ C/(v m), for pure water at 25°C. Under the assumption of a uniform fluid conductivity, the DC electric field $\mathbf{E}_{DC} = -\nabla\phi$ was computed by solving the Laplace equation $\nabla^2\phi = 0$ using the electrostatics module in COMSOL. The boundary conditions include the DC voltage drop between the channel ends and the insulating condition on the channel and constriction walls. The correction factor c for particle dielectrophoresis was determined by fitting the predicted particle trajectories to the width of the focused particle stream at the 10 kV/m DC electric field. The obtained c values for 5 and 10 μm particles were then used in all other electric fields including both pure DC and AC/DC cases.

5 Results and discussion

5.1 Particle focusing at various AC to DC electric field ratios

Figure 2 compares the experimentally obtained snap-shot (left column) and streak (middle column) images with the numerically predicted trajectories (right column) for the AC/DC dielectrophoretic focusing of 10 μm particles in the microchannel constriction. The total RMS magnitude of AC and DC electric fields was fixed to 10 kV/m while the AC to

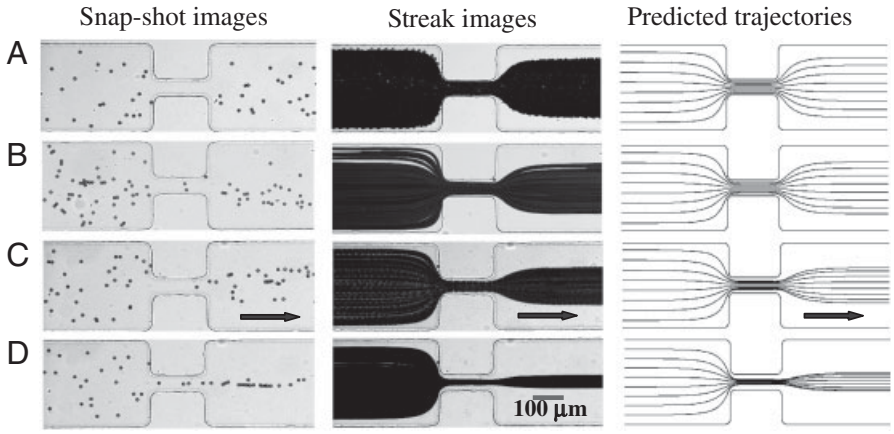

Figure 2. Dielectrophoretic focusing of 10 μm particles (left column: experimentally recorded snap-shot images; middle column: experimentally obtained streak images; right column: numerically predicted trajectories) in a microchannel constriction at various AC to DC electric field ratios: (A) $\alpha = 0$; (B) $\alpha = 1$; (C) $\alpha = 4$; (D) $\alpha = 9$. The total magnitude of the AC (1 kHz frequency) and DC electric fields was maintained at 10 kV/m. The block arrows indicate the flow directions.

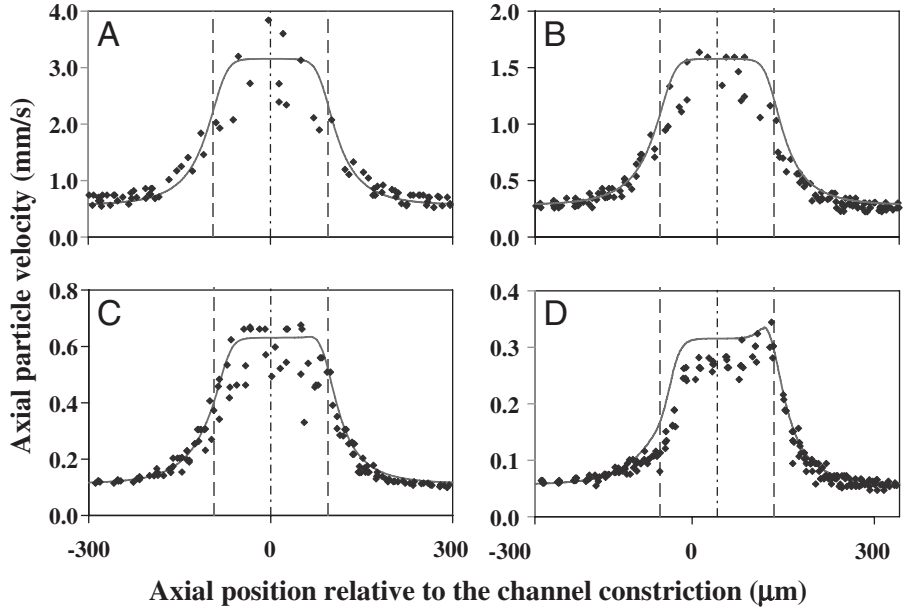

Figure 3. Velocity variations (curves for modeling results, symbols for experimental data) of 10 μm particles migrating along the centerline of a microchannel constriction at various AC to DC electric field ratios: (A) $\alpha = 0$; (B) $\alpha = 1$; (C) $\alpha = 4$; (D) $\alpha = 9$. The total magnitude of the AC (1 kHz frequency) and DC electric fields was maintained at 10 kV/m. The abscissas of all sub-plots indicate the axial positions with respect to the middle plane (*i.e.* the origins) of the constriction (*i.e.* the region between the two dashed vertical lines).

DC field ratio was varied from (a) $\alpha = 0$ or pure DC to (b) $\alpha = 1$ or 1DC/1AC, (c) $\alpha = 4$ or 1DC/4AC, and (d) $\alpha = 9$ or 1DC/9AC. In the simulations the correction factor c for the particle size effects on dielectrophoresis, see Eq. (13), remained constant at 0.4. For every electric field ratio α in Fig. 2, the predicted particle trajectories show a reasonable agreement with the recorded particle images. This justifies the use of the correction factor in the modeling. As analyzed above, particles are deflected to the channel center region by negative dielectrophoresis, leading to a narrower particle stream about the centerline in the downstream of the constriction. This dielectrophoretic focusing increases with the rise of AC to DC electric field ratio, α, as predicted in Eq. (12), which becomes apparent at $\alpha = 9$. We have uploaded four video clips (Supporting Information) corresponding to the particle focusing in the four cases displayed in Fig. 2.

Figure 3 shows the velocity variations (curves for modeling results, symbols for experimental data of at least five particles) of 10 μm particles migrating along the channel centerline (and thus the constriction centerline) at various AC to DC electric field ratios: (a) $\alpha = 0$; (b) $\alpha = 1$; (c) $\alpha = 4$; (d) $\alpha = 9$. The abscissas of all sub-plots indicate the axial positions with respect to the middle plane (see the origins) of the constriction (see the region between the two dashed vertical lines). One can see that other than the particle trajectories as demonstrated in Fig. 2, Eq. (13) also predicts reasonably well the particle velocity variations through the microchannel constriction. This agreement further justifies the use of the correction factor for dielectrophoresis in Eq. (13). As expected, particle velocity decreases linearly with α. At small values of α (including 0 and 1), the particle velocity profile is approximately symmetric about the constriction in Figs. 3A and B, indicating a relatively weak dielectrophoretic motion. This is consistent with the observed particle focusing behaviors in Figs. 2A and B. At $\alpha = 4$, the particle velocity profile is noticed to shift downstream with respect to the origin due to the dielectrophoretic retardation and propulsion in the upstream and downstream of the constriction, respectively. This shifting becomes even more obvious when α increases to nine. Moreover, there appears an extreme point in the particle velocity near the downstream edge of the constriction, the reason of which has been explained in Theoretical background, *i.e.* Section 2.

5.2 Particle focusing at various pure DC electric fields

In order to further demonstrate the advantages of using DC-biased AC electric fields in dielectrophoretic particle focusing, we investigated the particle focusing behaviors at various pure DC electric fields with the magnitude spanning from 10 to 100 kV/m. No higher fields were tested due to the concern of Joule heating [54] and other deleterious electrochemical reactions on the electrode surfaces [34]. Figure 4 compares the experimentally obtained snap-shot (left column) and streak (middle column) images with the numerically predicted trajectories (right column) for the DC dielectrophoretic focusing of 10 μm particles in the microchannel constriction. The magnitude of DC electric field was varied from (a) 10 to (b) 20, (c) 40, and (d) 100 kV/m. The correction factor c for the particle size effect on dielectrophoresis was still fixed at 0.4 in the simulations. Overall, the computed particle trajectories follow reasonably the observed particle focusing behaviors. As the magnitude of DC electric field increases, dielectrophoretic particle motion increases faster than electrokinetic motion due to the former's high-order dependence of electric field. Consequently, particles obtain a better focusing at larger electric fields as seen in Fig. 4 [see also Eq. (6)]. However, the width of the focused particle stream at the 100 kV/m DC electric field (see Fig. 4D) is only comparable with that at the 10 kV/m 1DC/9AC electric field (see Fig. 2D). In other words, a similar particle focusing can be realized at a much smaller magnitude if a DC-biased AC electric field is used.

5.3 Particle size effect on particle focusing

Given by Eq. (4), dielectrophoretic motion is proportional to the particle diameter squared. Hence, smaller particles should be focused more difficultly than larger ones. Figure 5

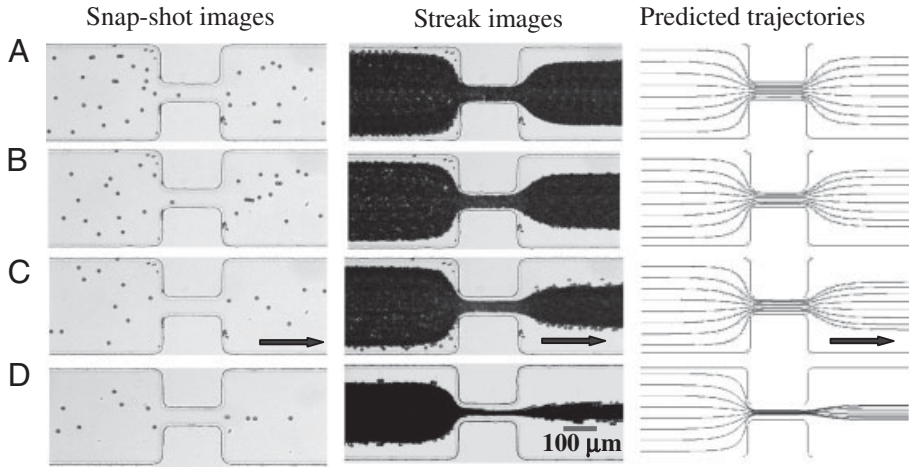

Figure 4. Dielectrophoretic focusing of 10 μm particles (left column: experimentally recorded snap-shot images; middle column: experimentally obtained streak images; right column: numerically predicted trajectories) in a microchannel constriction at various pure DC electric fields (*i.e.* the AC to DC electric field ratio is $\alpha = 0$): (A) 10 kV/m; (B) 20 kV/m, (C) 40 kV/m, and (D) 100 kV/m. The block arrows indicate the flow directions.

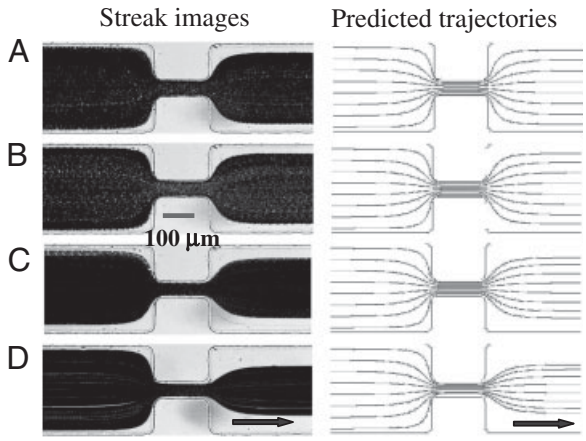

Figure 5. Dielectrophoretic focusing of 5 μm particles (left column: experimentally obtained streak images; right column: numerically predicted trajectories) in a microchannel constriction at various AC (1 kHz frequency) to DC electric field ratios: (A) $\alpha = 0$; (B) $\alpha = 1$; (C) $\alpha = 4$; (D) $\alpha = 9$. The total magnitude of the AC and DC electric fields was maintained at 10 kV/m. The block arrows indicate the flow directions.

illustrates the dielectrophoretic focusing of 5 μm particles through the microchannel constriction at various AC to DC electric field ratios: (a) $\alpha = 0$; (b) $\alpha = 1$; (c) $\alpha = 4$; (d) $\alpha = 9$. The total magnitude of the AC and DC electric fields was maintained at 10 kV/m. The correction factor c in Eq. (13) was set to 0.6. The numerically predicted particle trajectories (left column in Fig. 5) were found to agree with the experimentally obtained streak images (right column) for all electric field ratios. While the overall trend of enhancement in particle focusing with the rise of α is obvious in Fig. 5, the focused stream width of 5 μm particles at $\alpha = 9$ (see Fig. 5D) is barely close to that of 10 μm particles at $\alpha = 1$ (see Fig. 2B). In order to improve the dielectrophoretic focusing of small particles, one may simply increase the number of constrictions in the channel as the particle focusing effects through the constrictions are accumulative. It is also feasible to increase the magnitude of the total electric field and/or to reduce the width of the constriction though both approaches have their respective disadvantages as stated in the introduction.

6 Conclusions

We have studied the dielectrophoretic focusing of 5 μm and 10 μm polystyrene particles in a microchannel constriction using pure DC and DC-biased AC electric fields. It has been demonstrated that particles can be focused in a much smaller magnitude of electric field in the latter case due to the independent control of DC electrokinetic flow and AC/DC dielectrophoretic motion. This was verified by examining the width of the focused particle stream at different AC to DC electric field ratios. The effects of the DC electric field magnitude and particle size on particle focusing performance have also been examined. The obtained particle streak images and velocity variations through the microchannel constriction were both found to agree with the numerical predictions. Considering the increased flexibility and efficiency in particle handling and the decreased damage to bio-particles, we expect that DC-biased AC electric fields will find more applications in microfluidic particle-handling devices.

The support from Clemson University through a start-up package and a Research Equipment Fund to Xuan is gratefully acknowledged. He also appreciates the support from the State Key Laboratory of Nonlinear Mechanics in China.

The authors have declared no conflict of interest.

7 References

[1] Pamme, N., *Lab Chip* 2007, *7*, 1644–1659.

[2] Desai, J. P., Pillarisetti, A., Brooks, A. D., *Annu. Rev. Biomed. Eng.* 2007, *9*, 35–53.

[3] Tsutusi, H., Ho, C. M., *Mech. Res. Comm.* 2009, *36*, 92–103.

[4] Huh, D., Gu, W., Kamotani, Y., Grotgerg, J. B., Takayama, S., *Physiolog. Measur.* 2005, *26*, R73–R98.

[5] Chung, T. D., Kim, H. C., *Electrophoresis* 2007, *28*, 4511–4520.

[6] Ateya, D. A., Erickson, J. S., Howell, P. B., Jr., Hilliard, L. R., Golden, J. P., Ligler, f. S., *Anal. Bioanal. Chem.* 2008, *391*, 1485–1498.

[7] Lee, G. B., Chang, C. C., Huang, S. B., Yang, R. J., *J. Micromech. Microeng.* 2006, *16*, 1024–1032.

[8] Simonnet, C., Groisman, A., *Anal. Chem.* 2006, *78.l*, 5653–5663.

[9] Chang, C. C., Huang, Z. Y., Yang, R. J., *J. Micromech. Microeng.* 2007, *17*, 1479–1486.

[10] Tsai, C. G., Hou, H. H., Fu, L. M., *Microfluid. Nanofluid.* 2008, *5*, 827–836.

[11] Fu, L. M., Yang, R. J., Lee, G. B., *Anal. Chem.* 2003, *75*, 1905–1910.

[12] Yang, R. J., Chang, C. C., Huang, S. B., Lee, G. B., *J. Micromech. Microeng.* 2005, *15*, 2141–2148.

[13] Xuan, X., Li, D., *Electrophoresis* 2005, *26*, 3552–3560.

[14] Taylor, J., Stubley, G. D., Ren, C. L., *Electrophoresis* 2008, *29*, 2953–2959.

[15] Kohlheyer, D., Unnikrishnan, S., Besselink, G. A. J., Schlautmann, S., Schasfoort, R. B. M., *Microfluid. Nanofluid.* 2008, *4*, 557–564.

[16] Zhao, Y., Fujimoto, B. S., Jeffries, G. D. M., Schiro, P. G., Chiu, D. T., *Optics Express* 2007, *15*, 6167–6176.

[17] Shi, J., Mao, X., Ahmed, D., Colletti, A., Huang, T. J., *Lab Chip* 2008, *8*, 221–223.

[18] Takahashi, T., Ogata, S., Nishizawa, M., Matsue, T., *Electrochem. Commun.* 2003, *5*, 175–177.

[19] Lin, C. H., Lee, G. B., Fu, L. M., Hwey, B. H., *J. Microelectromech. Syst.* 2004, *13*, 923–932.

[20] Yu, C., Vykoukal, J., Vykoukal, D. M., Schwartz, J., Shi, L., Gascoyne, P. R. C., *J. Microelectromech. Syst.* 2005, *14*, 480–487.

[21] Cheng, I. F., Chang, H. C., Hou, D., Chang, H. C., *Biomicrofluidics* 2007, *1*, 021503.

[22] Tornay, R., Braschler, T., Demierre, N., Steitz, B., Finka, A., Hofmann, H., Hubbell, J. A., Renaud, P., *Lab Chip* 2008, *8*, 267–273.

[23] Yamada, M., Seki, M., *Lab Chip* 2005, *5*, 1233–1239.

[24] Aoki, R., Yamada, M., Yasuda, M., Seki, M., *Microfluid. Nanofluid.* 2009, *6*, 571–576.

[25] Choi, S., Song, S., Choi, C., Park, J. K., *Small* 2008, *4*, 634–641.

[26] Choi, C., Park, J. K., *Anal. Chem.* 2008, *80*, 3035–3039.

[27] Thwar, P. K., Linderman, J. J., Burns, M. A., *Electrophoresis* 2007, *28*, 4572–4581.

[28] Seo, J., Lean, M. H., Kole, A., *Appl. Phys. Lett.* 2007, *91*, 033901.

[29] Seo, J., Lean, M. H., Kole, A., *J. Chromatogr. A* 2007, *1162*, 126–131.

[30] Di Carlo, D., Irimia, D., Tompkins, R. G., Toner, M., *Proc. Natl. Acad. Sci. USA* 2007, *104*, 18892–18897.

[31] Di Carlo, D., Edd, J. F., Irimia, D., Tompkins, R. G., Toner, M., *Anal. Chem.* 2008, *80*, 2204–2211.

[32] Cummings, E. B., Singh, A. K., *Anal. Chem.* 2003, *75*, 4724–4731.

[33] Xuan, X., Raghibizadeh, S., Li, D. J., *Colloid. Interface Sci.* 2006, *296*, 743–748.

[34] Voldman, J., *Annu. Rev. Biomed. Eng.* 2006, *8*, 425–454.

[35] Kang, Y. J., Li, D. Q., Kalams, S. A., Eid, J. E., *Biomed. Microdev.* 2008, *10*, 243–249.

[36] Sabouncahi, P., Huber, D. E., Kanouff, M. P., Harris, A. E., Simmons, B. A., ''Joule heating effects on insulator-based dielectrophoresis,'' The 12th International Conference on Miniaturized Systems for Chemistry and Life Sciences (MicroTAS 2008), San Diego, CA, October 12–16, 2008.

[37] Lapizco-Encinas, B. H., Simmons, B. A., Cummings, E. B., Fintschenko, Y., *Anal. Chem.* 2004, *76*, 1571–1579.

[38] Lapizco-Encinas, B. H., Simmons, B. A., Cummings, E. B., Fintschenko, Y., *Electrophoresis* 2004, *25*, 1695–1704.

[39] Mela, P., van den Berg, A., Fintschenko, Y., Cummings, E. B., Simmons, B. A., Kirby, B. J., *Electrophoresis* 2005, *26*, 1792–1799.

[40] Pysher, M. D., Hayes, M. A., *Anal. Chem.* 2007, *79*, 4552–4557.

[41] Ozuna-Chacón, S., Lapizco-Encinas, B. H., Rito-Palomares, M., Martínez-Chapa, S. O., Reyes-Betanzo, C., *Electrophoresis* 2008, *29*, 3115–3122.

[42] Kang, K., Kang, Y., Xuan, X., Li, D., *Electrophoresis* 2006, *27*, 694–702.

[43] Keshavamurthy, S. S., Keonard, K. M., Burgess, S. C., Minerick, A. M., *NSTI-Nanotech* 2008, *3*, 401–404.

[44] Hawkins, B. G., Smith, A. E., Syed, Y. A., Kirby, B. J., *Anal. Chem.* 2007, *79*, 7291–7300.

[45] Lewpiriyawong, N., Yang, C., Lam, Y. C., *Biomicrofluidics* 2008, *2*, 034105.

[46] Morgan, H., Green, N. G., *AC Electrokinetic: Colloids and Nanoparticles*, Research Studies Press, Hertfordshire, UK, 2002.

[47] Ermolina, I., Morgan, H. J., *Colloid Interface. Sci.* 2005, *285*, 419–428.

[48] Santiago, J. G., *Anal. Chem.* 2001, *73*, 2353–2365.

[49] Kang, K., Xuan, X., Kang, Y., Li, D. J., *Appl. Phys.* 2006, *99*, 064702.

[50] Duffy, D. C., McDonald, J. C., Schueller, O. J. A., Whitesides, G. M., *Anal. Chem.* 1998, *70*, 4974–4984.

[51] Hunter, R. J., *Zeta potential in colloid science, principles and applications*. Academic Press, New York, 1981.

[52] Anderson, J. L., *Annu. Rev. Fluid Mech.* 1989, *21*, 61–99.

[53] Keh, H. J., Anderson, J. L., *J. Fluid. Mech.* 1985, *153*, 417–439.

[54] Xuan, X., *Electrophoresis* 2008, *29*, 33–43.

